Atmos. Chem. Phys., 25, 13123–13140, 2025 https://doi.org/10.5194/acp-25-13123-2025 © Author(s) 2025. This work is distributed under the Creative Commons Attribution 4.0 License.





Simulated mixing in the UTLS by small-scale turbulence using multi-scale chemistry-climate model MECO(n)

Chun Hang Chau, Peter Hoor, and Holger Tost

Institute for Atmospheric Physics, Johannes Gutenberg University Mainz, Mainz, Germany

Correspondence: Chun Hang Chau (cchau@uni-mainz.de) and Holger Tost (tosth@uni-mainz.de)

Received: 6 December 2024 – Discussion started: 20 December 2024 Revised: 30 August 2025 – Accepted: 1 September 2025 – Published: 21 October 2025

Abstract. The chemical composition of the upper troposphere and lower stratosphere (UTLS) plays an important role for the climate by affecting the radiation budget. Small-scale diabatic mixing like turbulence has a significant impact on the distribution of tracers which further affect the energy budget via their radiative impact. Current models usually have a higher vertical resolution near the surface and a coarser grid spacing in the free atmosphere, which is insufficient to resolve the occurrence of small-scale turbulence in the UTLS. In this work, we utilise enhanced vertical resolution (200 m in the UTLS) simulations focusing on mixing events in the Scandinavian region using the state-of-the-art multi-scale atmospheric chemistry model system MECO(n). These model simulations are able to represent different distinct turbulent mixing events in the UTLS and depict a significant impact of mixing on the tracer distribution in the UTLS. A novel diagnostic (delta tracer-tracer correlation) is introduced to determine the direction of the vertical mixing. The strength of the UTLS turbulent mixing depends on the particular situation, i.e., the vertical tracer gradient, and dynamical and thermodynamical forcing, i.e., vertical wind shear, deformation and static stability. This work provides evidence that high-resolution simulations are able to represent significant turbulent mixing in the UTLS region, allowing for further research on the UTLS turbulent mixing and its implications for the climate system.

1 Introduction

The upper troposphere and lower stratosphere (UTLS) is defined as the region around the tropopause which acts as a transition layer between the troposphere and stratosphere (Gettelman et al., 2011). The troposphere and stratosphere are fundamentally different in chemical composition and static stability, and they are separated by the tropopause, an immaterial surface acting as a vertical transport barrier. The dynamical tropopause (also known as the potential vorticity (PV) tropopause) is one of the commonly used definitions for the tropopause due to its conservation under isentropic conditions. The typical PV values for the dynamical tropopause can range from 1.6 PVU to 3.5 PVU, but 2 PVU is most commonly used (Stohl et al., 2003a). Since the PV tropopause is a quasi-impermeable surface for adiabatic frictionless flow, i.e., on isentropes, stratosphere-troposphere exchange (STE) across the tropopause may require diabatic

processes, e.g., like turbulent mixing by small-scale turbulence (Holton et al., 1995).

The distribution of chemical constituents and the resulting changes in the UTLS chemistry are a consequence of the complex atmospheric processes on various spatial and temporal scales (Riese et al., 2012). Bidirectional STE is one of the crucial processes affecting the chemistry of UTLS (Holton et al., 1995; Stohl et al., 2003b), especially in the extratropical transition layer (ExTL) in the extratropics (Gettelman et al., 2011).

The chemical composition of the UTLS plays an important role on the climate by affecting the radiation budget (Forster et al., 2021). Local changes in the tracer distribution in the UTLS will not only lead to local changes on the energy budget but also affect the surface climate (Riese et al., 2012; Lacis et al., 1990; Randel et al., 2007). Previous studies showed that the surface temperature is highly sensitive to the changing chemical composition in the UTLS region (Forster

and Shine, 1999, 2002). For example, changes in ozone distribution especially at the tropopause and lower stratosphere could have large impacts on the surface temperature (Forster and Shine, 1997). Besides the radiation budget, STE also has impacts on other aspects, such as stratospheric ozone recovery (Butchart and Scaife, 2001) and the tropospheric ozone budget (Lelieveld and Dentener, 2000).

Turbulent mixing is one of the processes of STE (Holton et al., 1995), especially in the region near the jet streams and tropopause folds (Shapiro, 1980). Clear air turbulence (CAT) is one of the major types of turbulence that occurs in the UTLS which could lead to rapid mixing of chemical species between stratosphere and troposphere (Esler and Polvani, 2004; Traub and Lelieveld, 2003). CAT refers to the turbulence in the free atmosphere that occurs in cloud-free regions or within stratiform clouds (Ellrod et al., 2003). It has a lifetime of 1 h to 1 d, with a typical vertical dimension from 500 to 1000 m (Overeem, 2002). Kelvin-Helmholtz instability (KHI) as a result of vertical shear of horizontal wind (Kunkel et al., 2019), forming a shear layer at the tropopause (Kaluza et al., 2021), is the major mechanism that leads to CAT formation (Watkins and Browning, 1973; Ellrod and Knapp, 1992). Consequently, CAT occurs when the vertical wind shear is strong enough to overcome the stable layer's inhibition (Williams and Joshi, 2013).

CAT occurs most frequently in the UTLS, especially near the tropopause (Dutton and Panofsky, 1970; Wolff and Sharman, 2008) and along the jet streams (Keller, 1990; Traub and Lelieveld, 2003). This phenomenon shows the highest probability of occurrence in boreal winter and is less frequent in boreal summer (Jaeger and Sprenger, 2007). An exceptional region is the eastern Mediterranean (Jaeger and Sprenger, 2007; Traub and Lelieveld, 2003) which is also known as a region with strong STE (Sprenger and Wernli, 2003).

Climate change is expected to increase the occurrence and intensity of CAT due to the strengthening of vertical wind shear (Williams, 2017), such that CAT is expected to have a large relative increase globally under the IPCC RCP 8.5 scenario, especially at the mid-latitudes (Storer et al., 2017). Williams and Joshi (2013) results suggested that if the atmospheric CO2 is doubled compared to the pre-industrial time, the strength of CAT in the North Atlantic during winter will increase by 10%-40% and the occurrence of CAT which is moderate or greater will increase by 40%-170%. Recent studies by Smith et al. (2023) and Hu et al. (2021) also show similar results over the North Atlantic and East Asia, respectively.

Considering the increasing trend of CAT, the link between turbulent mixing and STE, and hence the radiation budget, it is crucial to investigate the relation between CAT and mixing of chemicals in the UTLS. However, previous studies mainly focus on the dynamical aspect of turbulence (Kaluza et al., 2021; Muñoz-Esparza et al., 2020), but not on tracers. The main objective of this study is not to analyze the represen-

tation and strength of the turbulence itself but to systematically analyze the impact of turbulence on tracer mixing in the UTLS. For that purpose, a novel diagnostic, i.e., the delta tracer-tracer correlation is used within the multi-scale climate chemistry model MECO(n). Consequently, the main objective of the study is on the resulting effects on the tracer distributions caused by turbulent mixing. Note to differentiate between the mixing itself, i.e., the "dynamical" mixing represented by e.g., the turbulent kinetic energy (TKE), and the local effects on the tracer distributions provided by the mixing and the tracer gradient and further effects of the mixing, i.e., the downwind changes in the tracer distributions, originating from the mixing and subsequent processes, e.g., advection. The latter especially can further enhance vertical differences in tracer concentrations in the case of modified vertical gradients of the respective tracers.

The paper is structured as outlined below. Section 2 introduces the applied model, describes the model configuration and the novel diagnostic delta tracer–tracer correlation. Section 3 presents the results and discusses the details of the mixing by passive tracer tests conducted in this study. Section 4 summarizes the findings and draws conclusions.

2 Model description and methodology

This section gives a brief introduction to MECO(n) (Mertens et al., 2016), the EMAC and Consortium for Small-scale Modeling (COSMO) setup (including horizontal and vertical resolution, model domain and time step), the COSMO turbulence scheme, the explanation of the enhanced vertical grid for COSMO and the introduction of the novel diagnostic delta tracer—tracer correlation.

2.1 MECO(n) modeling system (v2.55.2)

MECO(n) represents the MESSy-fied (Modular Earth Submodel System, MESSy) European Centre Hamburg general circulation model (ECHAM) and COSMO models nested n times (Kerkweg and Jöckel, 2012a; Kerkweg et al., 2018), and is a state-of-the-art online coupled global/regional atmospheric chemistry model system based on the Modular Earth Submodel System (MESSy; Jöckel et al., 2005), which allows users to switch on or off physical and chemical processes through namelist interfaces. In MECO(n), the regional atmospheric model COSMO (Baldauf et al., 2011; Doms and Baldauf, 2018; Schättler et al., 2021) is nested online within the global general circulation model ECHAM5 (Roeckner et al., 2003); both COSMO and ECHAM5 are equipped with the MESSy infrastructure as individual COSMO/MESSy (Kerkweg and Jöckel, 2012b) and ECHAM/MESSy instances (EMAC; Jöckel et al., 2006, 2010). Besides the meteorological data, also the chemical composition and tracer information is exchanged between the individual instances. MECO(n) consequently allows an online coupling between different models so that the larger-scale (parent, e.g., EMAC or COSMO/MESSy) instance can provide the initial and boundary conditions for the smaller-scale (children, e.g., COSMO/MESSy) instances.

2.2 MECO(n) model configuration

In this study, MECO(n) contains two smaller nests besides the global instance: EMAC is coupled with an intermediate COSMO/MESSy instance (further denoted as CM40) and CM40 is further coupled with a target COSMO/MESSy instance (further denoted as CM10). EMAC is operated in T42L90MA (Giorgetta et al., 2006) resolution. It is a middleatmosphere configuration that has 90 vertical layers up to 0.01 hPa (approximately 80 km in altitude) at T42 horizontal resolution (approximately $2.8^{\circ} \times 2.8^{\circ}$ at the equator). The model time step is 360s and it is initialized with the ERA-Interim reanalysis data (Dee et al., 2011). EMAC has been weakly nudged (Jeuken et al., 1996) towards the ERA-Interim reanalysis data up to 10 hPa. The CM40 domain covers most of Europe from Spain and Iceland in the west to parts of Russia in the east with a horizontal resolution of 0.4° and a model time step of 120 s. The initial and boundary data are provided by the EMAC instance. The CM10 model region focuses on the Scandinavian region with a horizontal resolution of 0.1° and a model time step of 40 s. The initial and boundary data are provided by the CM40 instance. Both CM40 and CM10 have 84 vertical layers with an enhanced resolution in the UTLS, details of the enhanced grid are discussed in Sect. 2.4.

2.3 Vertical mixing in COSMO

The mixing in the COSMO model is divided into two parts: (1) small-scale turbulent diffusion, and (2) organized moist convection. In this study, we focus on the impact of the small-scale turbulent diffusion. In COSMO, the subgrid-scale turbulent diffusion is based on K-theory, the constitutive equation is as follows:

$$F_{\psi} = -K_{\psi} \cdot \nabla \psi. \tag{1}$$

This equation relates the subgrid-scale turbulent flux of a scalar quantity F_{ψ} to the gradient of ψ and a diffusion coefficient K_{ψ} . The determination of the K_{ψ} depends on the chosen turbulent closure scheme. COSMO provides two different turbulent schemes. The default setup uses a 1-D diagnostic closure scheme by Muller (1981). In this scheme, K_{ψ} is determined by the Blackadar length scale (Blackadar, 1962), vertical wind shear, Brunt–Väisälä frequency and stability functions which are based on the flux-Richardson number. However, this scheme comes with several drawbacks including insufficient vertical mixing in stable stratification. COSMO also provides another newer turbulent scheme based on prognostic turbulent kinetic energy. The K_{ψ} in this prognostic TKE-based scheme is in the forms

$$K^{\rm H} = q\lambda S^{\rm H},\tag{2}$$

$$K^{M} = q\lambda S^{M}, \tag{3}$$

where $K^{\rm H}$ and $K^{\rm M}$ are the turbulent diffusion coefficients for heat and momentum respectively. They are computed by the corresponding stability functions for scalars ($S^{\rm H}$) and for momentum ($S^{\rm M}$) which are determined by the flux-Richardson number, the turbulent length scale λ (which is assumed to be the Blackadar mixing length) and the turbulent velocity scale $q = \sqrt{2e_t}$, where $\overline{e_t}$ is the TKE. The latter scheme is used in this study. Details for the turbulent schemes can be found in Sect. 3 (Sect. 3.3.2 for the used scheme) of the COSMO model documentation by Doms et al. (2018).

2.4 Enhanced vertical grid for COSMO instances

The default vertical grid for COSMO is either 40 or 50 levels that reach up to 22 km, with an 11 km damping layer starting at 11 km. Furthermore, these default vertical grids have a finer resolution near the surface and a coarser resolution in the free atmosphere, which makes the default setup too low and too coarse for resolving small-scale turbulence or other processes in the UTLS. Previous studies also show that STE-related processes are sensitive to the model resolution (Miyazaki et al., 2010; Meloen et al., 2003; van Velthoven and Kelder, 1996). In MECO(n), the model TKE is sensitive to the vertical resolution and the mixing strength is sensitive to both horizontal and vertical resolution (details in the Supplement). Therefore, in this study, we introduce an enhanced vertical grid focused on the UTLS which is applied to both CM40 and CM10. It is modified from an established extended vertical grid (Eckstein et al., 2015) with 60 levels (further denoted as EX-60) which reaches the lower stratosphere up to 33 km, with a 5 km damping layer starting at 27 km. Our enhanced setting has 84 levels and also reaches up to 33 km, with an identical 5 km damping layer starting at 27 km considering that Eckstein et al. (2015) show that the differences between 5 and 11 km damping layers are marginally small, and the analysis carried out in this study are far below the damping layer with more than 20 model levels, the potential reflection from the model top should be negligible. In order to reduce modifications of the boundary layer due to the change of vertical grid, we kept the levels below 8 km unchanged and only increase the resolution between 8 and 15 km to 200 m per level considering the typical size of CAT (Overeem, 2002). The level definition for the default 40 levels (further denoted as D-40), 50 levels (further denoted as D-50), EX-60 and the enhanced vertical grid (further denoted as EH-84) are shown in Fig. 2. EH-84 is evaluated with ERA5 data as well as comparisons with the tested EX-60 setup.

EH-84 is able to simulate the atmosphere reasonably. Although there is some discrepancy, the temperature pattern from ERA5 is generally well produced by the model as well as the relative humidity. There is a systematic cold bias in the CM10 output. However, the systematic cold bias that occurs in EH-84 is also found in EX-60 as well as the CM40

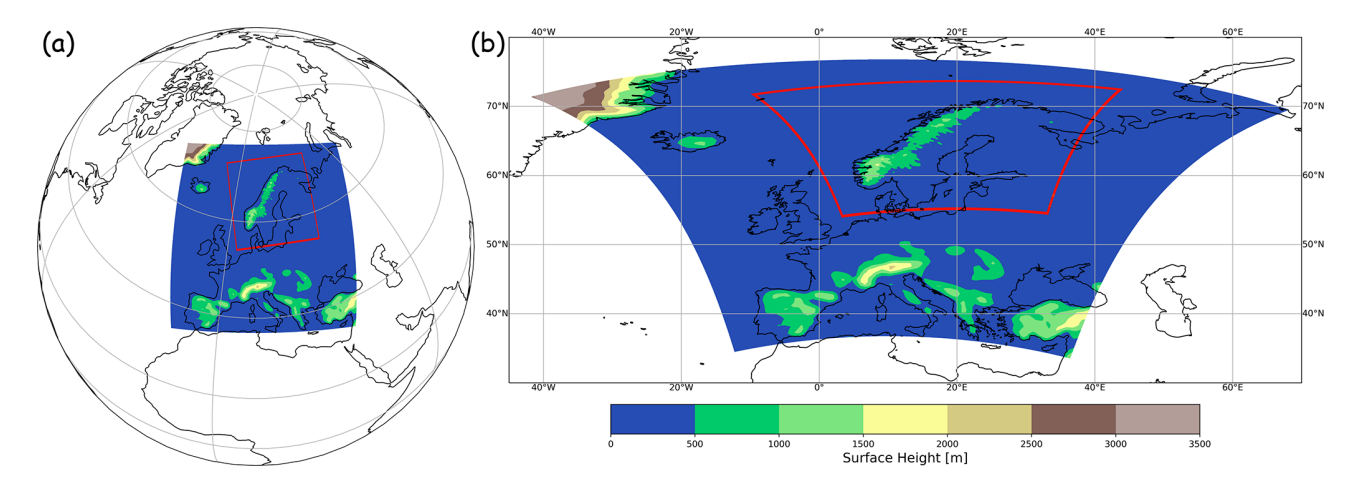


Figure 1. Model domain for MECO(n) with surface height: (a) an overview and (b) a close-up for CM40 and CM10.

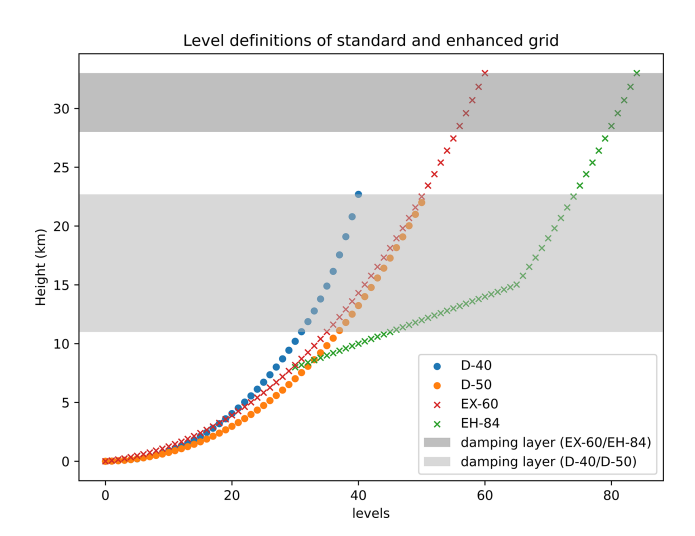


Figure 2. The vertical level definition of D-40, D-50, EX-60 and EH-84 vertical grid, the shaded area represents the damping layer of the respective vertical grid.

and EMAC output, indicating that the occurrence of the cold bias is not a result of the increased vertical resolution in the UTLS. There is a strong alignment of the main meteorological parameters between the EH-84 and EX-60 output, and the latter is well evaluated against observations (Eckstein et al., 2015). Consequently, the model output from the enhanced vertical grid EH-84 can be seen as reliable and suitable for the needs of this study. Details of the evaluation of EH-84 can be found in the Supplement. Furthermore, a sensitivity study was conducted in the Supplement to show the necessity of higher vertical and horizontal resolution. The occurrence of high TKE values in EH-84 is more frequent than in EX60 (Fig. S9), hence the mixing is more frequent (Figs. 8 and S11). CM10 (Fig. 8) also shows more efficient mixing than CM40 (Fig. S12) despite the similar TKE frequency.

2.5 Delta tracer-tracer correlation

In order to investigate the tracer mixing in the UTLS, we introduced a novel diagnostic, namely a delta tracer-tracer correlation, which is a similar concept to the tracer-tracer correlation, but makes use of the model capabilities. While the tracer-tracer correlation can be compared to the real world, the delta tracer-tracer correlation is a correlation between the differences of the tracers from model experiments. Instead of showing the mixing as an accumulation affected by other processes, it shows the impact of a single process (and potential subsequent advection differences). It requires two pairs of tracers (one pair of stratospheric and one pair of tropospheric). The difference of each pair, is a particular process being deactivated on one of the tracers in the model to investigate the impact of it. In our study, it is the turbulent vertical diffusion (vdiff). The detailed released tracers are described in Sect. 3.2. The delta tracer-tracer correlation can also be used to determine the direction of vertical mixing. Several distributions are expected for different scenarios: (1) concentrated distribution at the center [0,0] if no vertical mixing takes place at all; (2) diagonal distribution for bidirectional mixing, where both tracers change at a similar rate, causing the data point spread along the diagonal. The bidirectional mixing could be either balanced or imbalanced, meaning an even (case 1, spread equally from the center [0,0]) or uneven (case 2, spread unequally from the center [0,0]) spread along the diagonal. Balanced bidirectional mixing indicates a similar amount of stratospheric tracers being exchanged with the tropospheric tracers, while imbalanced bidirectional mixing indicates a different amount of stratospheric tracers being exchanged with the tropospheric tracers. It could be attributed to different situations, details are discussed in the following cases. The upper left section of the diagram indicates the downward mixing of stratospheric tracers into the troposphere since at the same grid, there are increasing stratospheric tracers and decreasing tropospheric tracers. And the lower right quadrant indicates the opposite, with decreasing stratospheric tracers and increasing tropospheric tracers, i.e., upward mixing of the tropospheric tracers. Scatter further away from the center indicates irreversible mixing, as the composition of the air masses is substantially modified, and the tracer is mixed irreversibly into the grid, i.e., instantaneously horizontally mixed. Additionally, this scatter is caused by initial differences from the mixing which are then amplified by (mostly horizontal) advection into regions where the vertical gradient of the tracers are different. Those different gradients can originate both from the tracer mixing event itself further upstream or from specific meteorological conditions, e.g., tropopause folds with strong gradients. Scatter away from the diagonal (case 3) indicates that the mixing occurs in a region with a different tracer gradient, a non-local effect introduced by other processes like horizontal advection acted on the mixed tracer. The scatter away from the diagonal gives an indication that the mixing is non-local, but the strength of mixing itself is still solely contributed by the turbulent mixing.

3 Results and discussion

3.1 Turbulence in the UTLS

Considering that turbulence in EMAC is dampened in the free atmosphere due to its hydrostatic characteristic and the formulation of the turbulence scheme (designed for the boundary layer only), this section analyzes how well the COSMO instances are able to represent turbulence and associated mixing. Therefore, the model TKE is compared with a calculated turbulence index using the grid-scale wind data from COSMO, i.e., the turbulence diagnostic TI1 from Ellrod and Knapp (1992), which includes a vertical wind shear term and a deformation (stretching and shearing) term to examine whether the highly parameterized subgrid-scale turbulence scheme is consistent with the grid-scale wind. The calculated TI1 is divided into five categories (i.e., null, light, moderate, severe and extreme) according to the thresholds set by Sharman et al. (2006). The features of the turbulence including the distribution and relative strength are reproduced by the COSMO instance as can be seen in Figs. 3 and 4, which shows the calculated TI1 (Fig. 3) and model TKE (Fig. 4) on the selected vertical levels, respectively. The TI1 generally agrees with TKE in terms of distribution and relative strength. The discrepancy between them might be caused by the neglected mechanisms of the Ellrod index or other subgrid-scale processes that could potentially lead to the formation of turbulence in the UTLS, e.g., subgrid-scale gravity waves. The high TKE and Ellrod index shown in Figs. 3 and 4 is caused by the jet stream as shown in Fig. S18. The increased shear could be attributed to the higher vertical and horizontal resolution, as shown in Fig. S19. CM10 shows a finer structure and hence more shear. It is important to note that the Ellrod index does not fully represent the turbulence in the atmosphere since it does not account for all producing mechanisms. For example TI1 might neglect the shear related to anticyclonic flow (Ellrod and Knox, 2010). It is also important to note that the comparison between the TI1 and TKE is not sufficient enough considering both of them are calculated from the COSMO wind field; comparison with observation should be conducted when there is available data. In addition, the strength between TI1 and TKE is not directly comparable since the TI1 threshold was set according to the verbal report of pilots and is subjective to the pilot's feelings and there is no similar threshold available for TKE. However, the results at least show consistency in the distribution on different levels. To conclude, the model grid-scale wind field is consistent with the model turbulence scheme and can detect the occurrence of turbulence in the model.

We also compare the model results with the last flight in the GW-LCYCLE II campaign (Witschas et al., 2023) on 1 February in northern Scandinavia. We derive a measure of turbulence from the high-frequency measured N₂O (Lachnitt et al., 2023) and link it with the model TKE. We computed a 31-point running standard deviation normalized with the variability of the window for N₂O. The running standard deviation shows the N₂O fluctuation from the background in a short period of time, while the normalization eliminates the effect of a tracer gradient due to the changing flight altitude or large-scale exchange of air masses. Figure 5 shows the model TKE at the flight time with the normalized running standard deviation of the measured N₂O. It shows that the derived turbulence signal often coincides well with the simulated TKE (Fig. 5a), the stronger signals (higher percentiles, Fig. 5b) coincide with the higher model TKE as well. This indicates that there is a reasonable degree of consistency between the derived turbulence signal from the measured N2O with the simulated turbulence.

3.2 Passive tracer test

In order to investigate the ability of mixing by turbulence in MECO(n), a series of passive tracer tests is performed by initializing several pairs of passive tracers in the simulation via the MESSy submodel PTRAC (Jöckel et al., 2008). The PTRAC submodel allows users to define the physical and chemical properties of specific tracers. In this study, we define a total of four pairs of artificial passive tracers with different distributions and slightly different physical properties. For the same pair of tracers, the only difference is whether the physical process of vertical diffusion (vdiff) is turned on or off. The vertical diffusion was switched off at the very beginning. An O₃-like tracer with a relatively steep linear gradient and a N2O-like tracer with a relatively gentle gradient are initialized to investigate the effect of the tracer gradient on the strength of mixing under a relatively realistic scenario. The tracers change linearly at the transition layer near the tropopause between approximately 300 and 100 hPa. The initial condition of the tracers is shown in Fig. S20 as a ver-

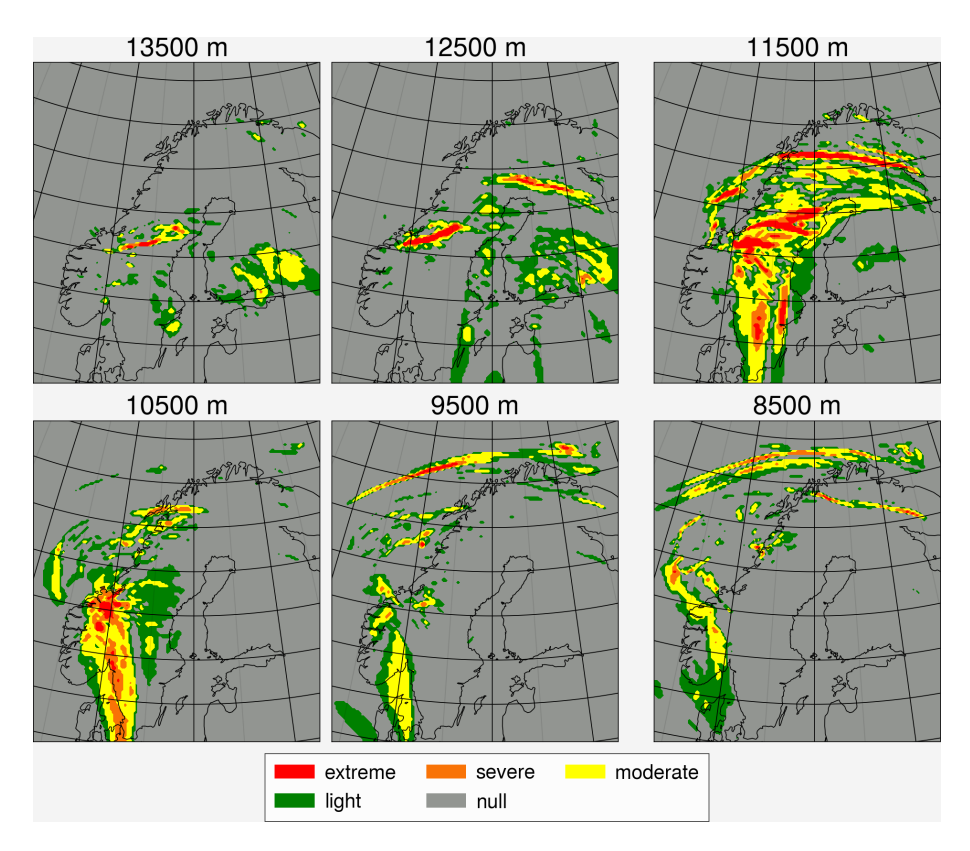


Figure 3. Calculated turbulence index (TI1) on 7 February 2016 at 20:00 UTC: null: grey, green: light, yellow: moderate, orange: severe, red: extreme.

Table 1. Summary of the released passive tracers.

Pair no.	Tracer	vdiff (on/off)	Mixing ratio [mol mol ⁻¹]	Stratospheric/tropospheric
1	O ₃ -like	on	2.4×10^{-8} to 4.0×10^{-6}	Stratospheric
1	O ₃ -like	off	2.4×10^{-8} to 4.0×10^{-6}	Stratospheric
2	N ₂ O-like	on	3.2×10^{-7} to 6.4×10^{-8}	Tropospheric
2	N ₂ O-like	off	3.2×10^{-7} to 6.4×10^{-8}	Tropospheric
3	Inverted O ₃ -like	on	4.0×10^{-6} to 2.4×10^{-8}	Tropospheric
3	Inverted O ₃ -like	off	4.0×10^{-6} to 2.4×10^{-8}	Tropospheric
4	Inverted N ₂ O-like	on	6.4×10^{-8} to 3.2×10^{-7}	Stratospheric
4	Inverted N ₂ O-like	off	6.4×10^{-8} to 3.2×10^{-7}	Stratospheric

tical profile. In order to investigate the direction of mixing, inverted versions of both tracers are also released in order to have stratospheric and tropospheric tracers with a similar gradient at the same time. A summary of the tracers is shown in Table 1.

3.3 Results: case studies

3.3.1 Case 1: turbulence induced balanced bidirectional mixing in a stable region

Case 1 (Fig. 6) is located within a typical high-level ridge trough system over Europe in the transition region between

the anticyclonic ridge and the cyclonic trough, with the potential for strong wind shear and convergence. It is also associated with the jet stream, regions with relatively low *Ri* are found at the vicinity of the tropopause and the core of the jet stream (Fig. 7).

Figure 8 shows the cross section of the distribution (top) and differences (bottom; vdiff on – vdiff off) for the O_3 -like (right) and inverted O_3 -like (left) tracers. The results show that vertical turbulent diffusion has a significant impact on the tracers. For the tropospheric inverted O_3 -like tracers, a higher mixing ratio above the tropopause and a lower mixing ratio below the tropopause is simulated when vertical turbu-

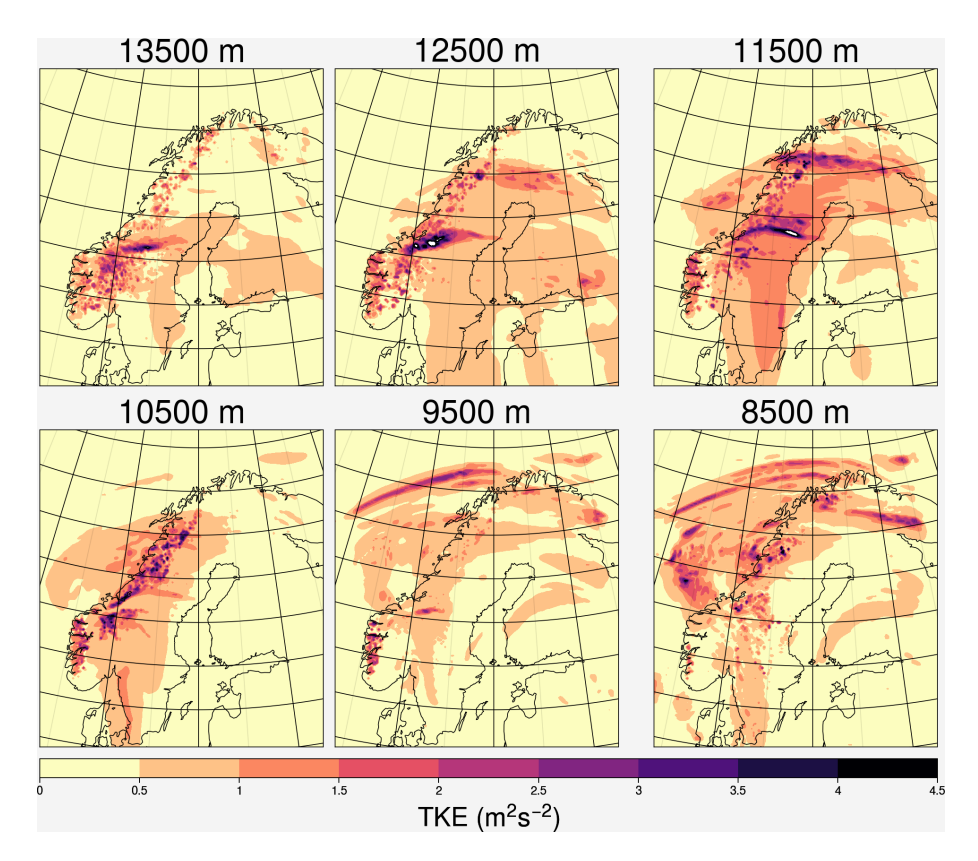


Figure 4. Model turbulence kinetic energy (TKE) on 7 February 2016 at 20:00 UTC.

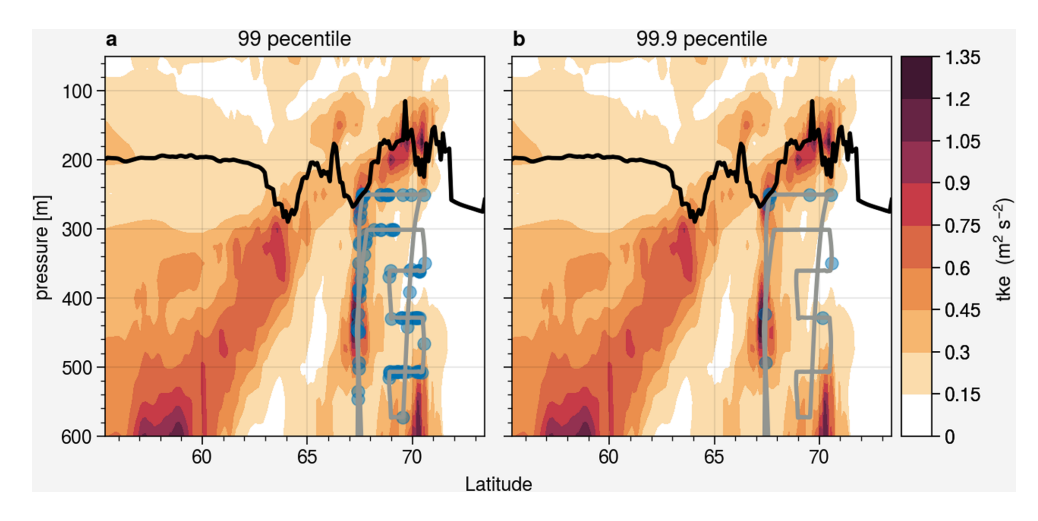


Figure 5. Cross section of average model TKE during the flight time. The black line represents the PV tropopause, the grey line represents the flight track, and the scatters represent the (a) 99th percentile and (b) 99.9th percentile of the normalized running standard deviation, i.e., the regions where the N_2O shows high normalized variability, potentially due to turbulence.

lent diffusion is present. This indicates that the tracers were transported across the tropopause by turbulent mixing from the troposphere to the stratosphere. The stratospheric O₃-like tracer shows analogous behavior but in an inverse manner, in which the turbulent mixing shifts the tracers from the stratosphere into the troposphere. By comparing the differences

with the background mixing ratio, vertical mixing could lead to almost 10% of differences near the tropopause. Similar mixing behavior is also noticeable for the N_2O -like and inverted N_2O -like tracers but in a weaker form (approximately 5%) due to its relatively gentle gradient (Fig. S8). Note that the tracer differences are strongest, exactly in the region with

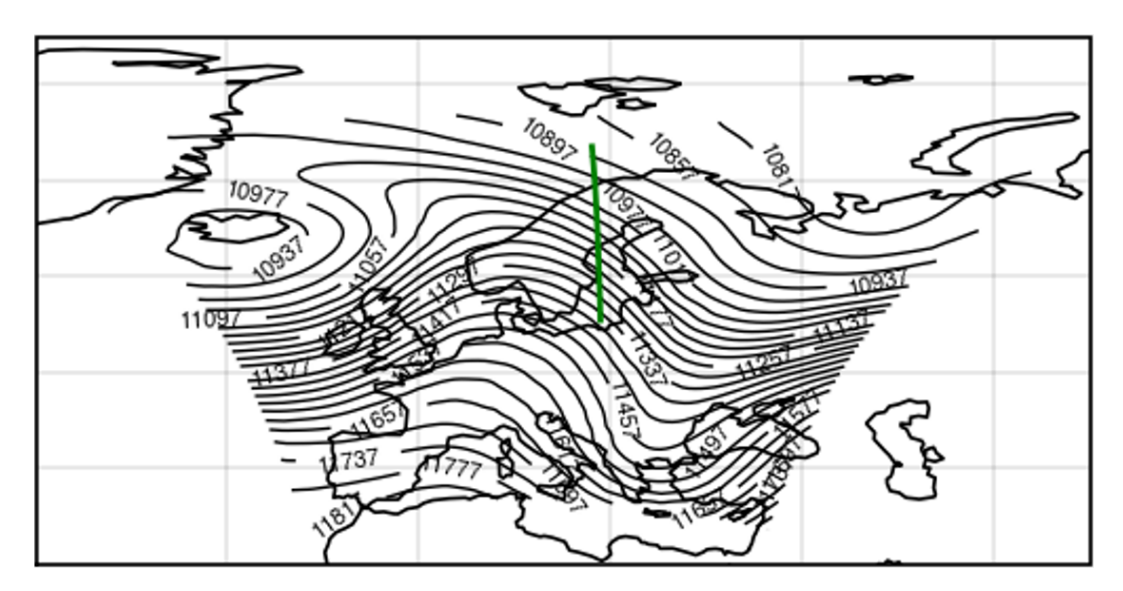


Figure 6. Case 1: geopotential height (gpm) at 200 hPa from CM40 on 5 February 2016 at 18:00 UTC. Green line indicates the location of the selected cross section of case 1.

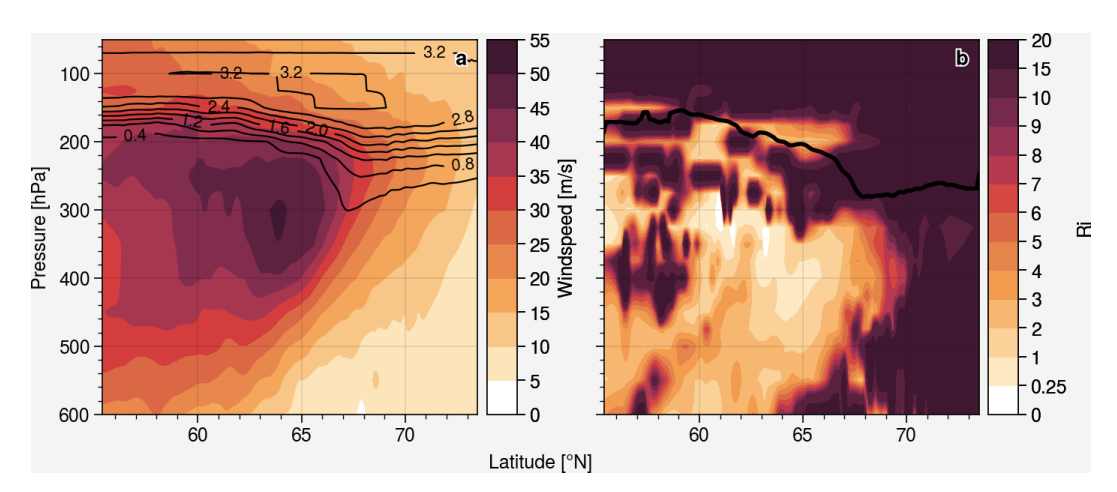


Figure 7. Case 1: (a) CM10 horizontal wind speed, the black contour line show the O_3 -like tracer and (b) gradient Richardson number (Ri), the black line indicates the PV tropopause.

the lowest gradient Richardson number (cf. Figs. 7b and 8c, d), indicating turbulence as the origin of the high spatial correlation.

Figure 9 shows the tracer–tracer correlation for different pairs of passive tracers at the same time and location as the cross section of Fig. 8. Figure 9a and b show a tracer–tracer correlation between the O_3 -like stratospheric tracer and N_2O -like tropospheric tracer with and without vertical diffusion respectively. Considering the passive tracers were released with a linear gradient, the tracer–tracer correlation shows a linear distribution as well, unlike the other classic tracer–tracer correlation which normally has an exponential relationship. Perfect correlation with diagonal distribution is expected if vertical diffusion does not play any role in transporting the tracer. Considering the magnitudes of the mix-

ing ratio in both tracers, the difference is hard to distinguish for a single mixing event of Fig. 8 in the tracer–tracer correlation. Therefore, the tracer–tracer correlation of the same tracer with and without vertical diffusion was performed as well. Figure 9c and d show the correlation with and without vertical diffusion for the stratospheric O_3 -like and tropospheric N_2O -like tracer respectively. Both tracers show some dispersion from the diagonal, indicating that vertical diffusion is affecting the tracers, leading to a deviation from perfect correlation. In addition, a delta tracer–tracer correlation (see Fig. 2.5 for an explanation of this diagram) is performed for O_3 -like and N_2O -like tracers.

Figure 10 shows the color-coded delta tracer-tracer correlation for the stratospheric O₃-like/inverted tropospheric O₃-like tracers of the mixing event on 5 February 2016 at

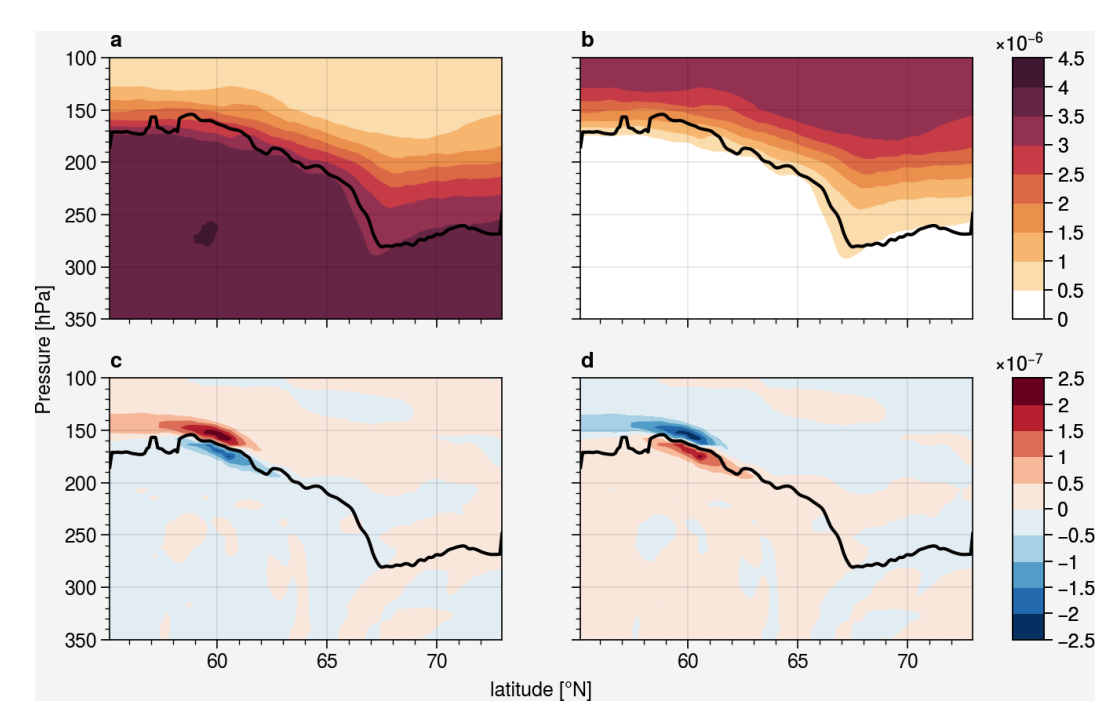


Figure 8. Cross section of the distribution: (a) inverted O_3 -like tracers (mol mol⁻¹), (b) O_3 -like tracers (mol mol⁻¹); and (c) difference (vdiff on – off) of the inverted O_3 -like tracers (mol mol⁻¹), (d) difference of the O_3 -like tracers (mol mol⁻¹) on 5 February 2016 at 18:00 UTC. The black line indicates the PV tropopause.

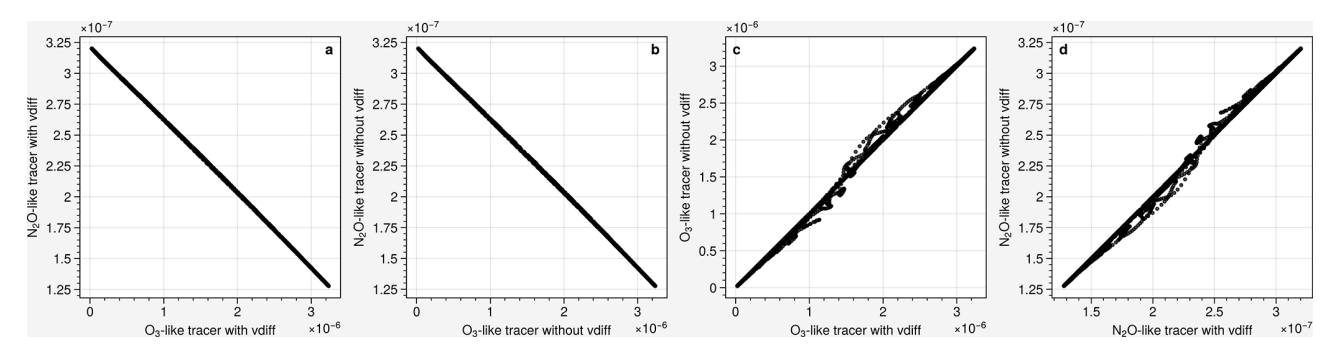


Figure 9. tracer–tracer correlation for (a) O_3 -like/ N_2O -like tracers with vdiff (mol mol⁻¹); (b) O_3 -like/ N_2O -like tracers without vdiff (mol mol⁻¹); (c) O_3 -like tracers with/without vdiff (mol mol⁻¹), (d) N_2O -like tracers with/without vdiff (mol mol⁻¹) on 5 February 2016 at 18:00 UTC.

18:00 UTC (Fig. 8). It is conducted using every grid point between 100 and 350 hPa at the indicated location on Fig. 6. It is a bidirectional mixing event associated with turbulence, which shows a diagonal distribution, indicating that at a specific location, the change of stratospheric tracer is similar to the change of tropospheric tracer. The symmetric distribution indicates that the mixing is balanced in strength in both directions. The strong downward mixing of the stratospheric air is caused by vertical wind shear or/and deformation: the region with strong downward mixing is concurrently the region with extreme turbulence according to the Ellrod index, as well as the strong vertical wind shear (VWS), deformation and relatively high TKE values. Considering that the vertical wind

shear and deformation are the key mechanisms for turbulence formation, and vertical wind shear is related to the calculation of TKE, it is reasonable that they show similar behavior. For static stability, the Brunt–Väisälä frequency (N^2) shows no distinct behavior, with most of the region reaching the typical stratospheric value. These characteristics of the mixing event are consistent with the findings by Kaluza et al. (2021), where strong vertical wind shear is able to be maintained under stable conditions. The strong upward mixing of the tropospheric air cannot be easily attributed to the vertical wind shear or deformation. Although light turbulence occurs in the strong upward mixing regions, the same strength of mixing as the downward flow cannot be explained. According to the

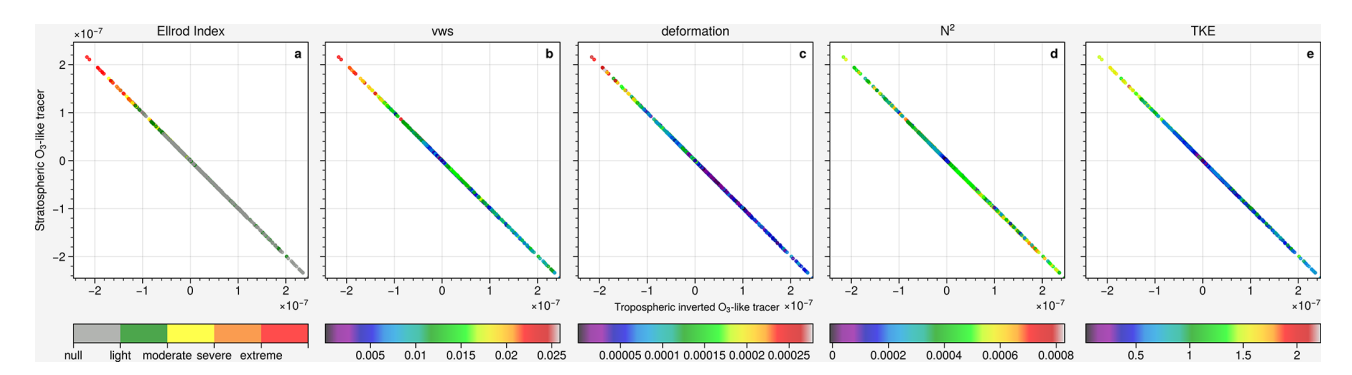


Figure 10. Case 1: Delta tracer–tracer correlation for determining the direction of vertical mixing of stratospheric O_3 -like/inverted tropospheric O_3 -like tracers (mol mol⁻¹) color-coded with (a) Ellrod index (s⁻²), (b) vertical wind shear (s⁻¹), (c) deformation (s⁻¹), (d) Brunt–Väisälä frequency (s⁻²), and (e) turbulence kinetic energy (m² s⁻²) on 5 February 2016 at 18:00 UTC.

constitutive equation of vertical diffusion in Fig. 2.3, the turbulent flux of tracers is calculated by the diffusion coefficient and the gradient of the tracer. Besides the diffusion coefficient, which is determined by the dynamics and thermodynamics of the atmosphere, the tracer gradient also plays a role on the mixing strength, such that mixing in a homogeneous atmosphere will have no effects on the tracers no matter how strong the mixing coefficient would be. In order to investigate the impact of the tracer gradient, the mixing is normalized by the tracer gradient to remove its impact. Figure 11 shows the same delta tracer-tracer plot but color-coded with absolute value of the difference of the stratospheric O₃-like tracer (left, |dO₃ST|) and absolute value normalized with the tracer gradient (right, |dO₃ST|/|gradient|). The downward mixing attributed to the dynamical forcing remained strong after normalization, while the upward mixing with much weaker dynamical forcing became weaker compared to the downward flow after normalization, showing that the upward flow could be attributed to the tracer gradient.

3.3.2 Case 2: imbalanced bidirectional mixing

Case 2 (Fig. 12), again located within a typical high-level ridge trough system over Europe instead of within the transition region as in case 1, is closer to the ridge axis. It is also associated with the jet stream, region with relatively low *Ri* are found at the vicinity of the tropopause and jet stream (Fig. 13).

Figure 14 shows a similar plot to Fig. 10, however, this time for an imbalanced bidirectional mixing event on 5 February 2016 at 05:00 UTC. The graph also shows a diagonal distribution, but asymmetrically. The lower right have a significantly shorter range than the upper left (unlike Case 1, which has a similar range on both ends). This indicates that in this specific profile, the changes in stratospheric air are different from the tropospheric air. This is a consequence of asymmetric stability and flow conditions, i.e., the stable layering of the stratosphere prevents deeper mixing into the stratosphere, whereas the lower static stability in the tropo-

sphere allows for deeper penetration of stratospheric tracers into the troposphere (where in Fig. 14d the lower right with high N^2 has a shorter range than the upper left with low N^2 , while Fig. 10d of case 1 has a similar N^2 on both ends).

The mixing strength in this case is relatively weak compared to the other cases. The stronger downward mixing of stratospheric air could again be attributed to the relatively strong vertical wind shear and deformation, most of the region with downward mixing is at least experiencing light to moderate turbulence. The low static stability also plays a role in the stronger downward mixing.

The region with weaker upward mixing exhibits noticeably weaker vertical wind shear and deformation compared to the region with downward mixing. The atmosphere is also much more stably stratified than the region with strong downward mixing (the N^2 is distinctly higher in this region). The upward mixing tropospheric air is therefore weaker because the weak dynamical instability is suppressed by the strong static stability.

3.3.3 Case 3: mixing associated with strong vertical gradient

Case 3 (Fig. 15) is located at the outflow region of the high-level trough ridge system, with potential of strong divergence. It is also the only case that the jet stream was shifted outside of the CM10 model domain, causing it to be relatively stable compared to the other two cases (Fig. 16).

Figure 17 shows another mixing event associated with strong vertical gradient on 3 February 2016 at 22:00 UTC. The mixing again shows a diagonal and symmetric distribution but with more scatter from the diagonal. This means, that the mixing does not only lead to equal changes in the tracer distributions, but more to entries of tropospheric tracers into regions of typically stratospherically dominated regimes. The scatter away from the diagonal, unlike the other two cases, where the modeled TKE is better correlated with the mixing (not shown), is due to the advection, the mixing shown in Fig. S17 and S22 located at the downwind re-

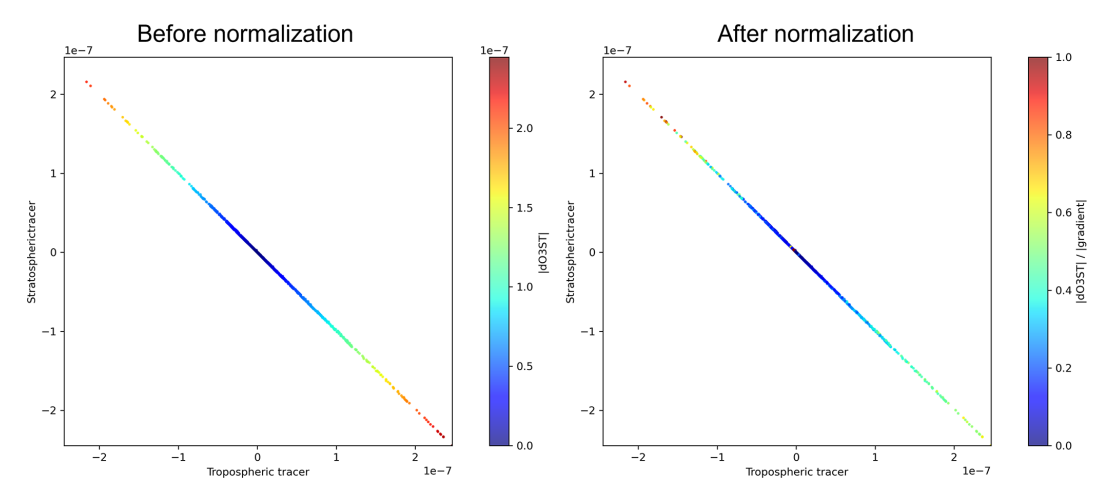


Figure 11. Delta tracer-tracer correlation color-coded with |dO₃ST| (mol mol⁻¹; left) and |dO₃ST|/|gradient| (right).

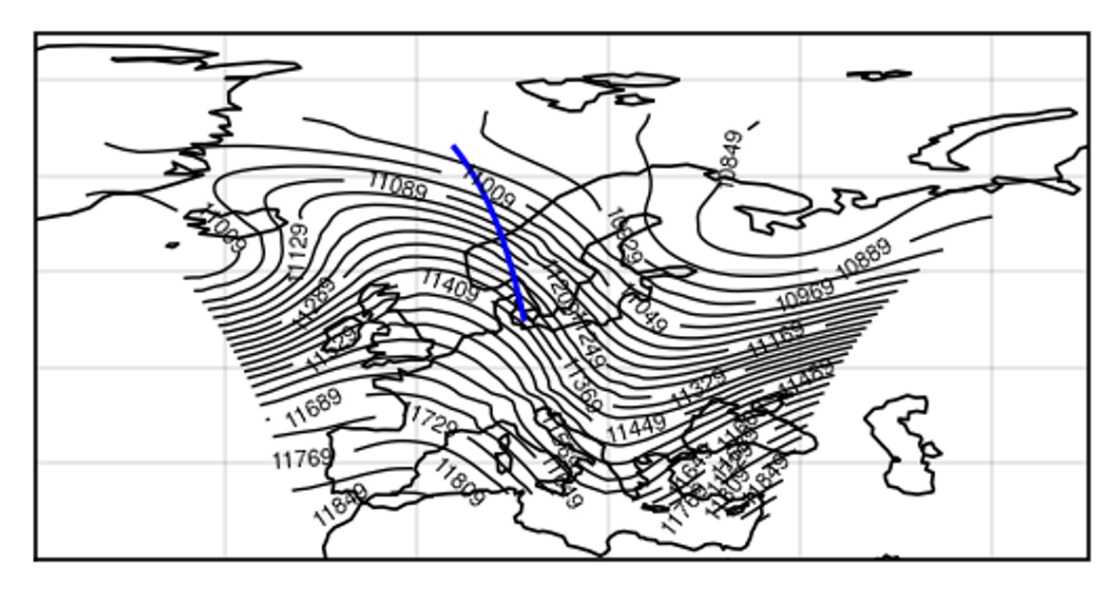


Figure 12. Case 2: geopotential height (gpm) at 200 hPa from CM40 on 5 February 2016 at 05:00 UTC. The blue line indicates the location of the selected cross section of case 2.

gion of the high TKE region (Fig. S21). In the earlier time, the mixing region (Fig. S22, left panel) is more co-located with the high TKE region (Fig. S21, left panel). After several hours, the mixing region (Fig. S22, right panel) propagates to the downwind region, while the high TKE region (Fig. S21, right panel) remains at the same location. The strong horizontal advection in the region of strong horizontal gradients changes the background ratios in addition to the vertical mixing and thus introduces additional mixing during each time step compared to the other cases. The wider the scatter is, the more, e.g., tropospheric tracer depletion is found at similar stratospheric tracer values.

However, in contrast to case 1, the dynamical and thermodynamical forcing do not play a key role in this case. The Ellrod index shows nearly no turbulence at all, neither vertical wind shear nor deformation shows any distinct behavior as in case 1. The static stability does not reach very high values in the stratosphere, such that the mixing is almost equally balanced.

3.3.4 Case inter-comparison

In order to examine whether the tracer gradient is responsible for the strength of the mixing events, the mixing is again normalized by the tracer gradient. Figures 18 and 19 show the frequency distribution for all 3 cases before (|mixing|) and after (|mixing|/|gradient|) normalization. Cases 1 and 3 have similar strength on mixing while case 2 is significantly weaker. Moreover, Cases 1 and 2 have similar distributions on dynamical forcing whereas case 3 forcing is notably weaker. After normalization, the mixing of Case 3 becomes much weaker considering the dynamical forcing does

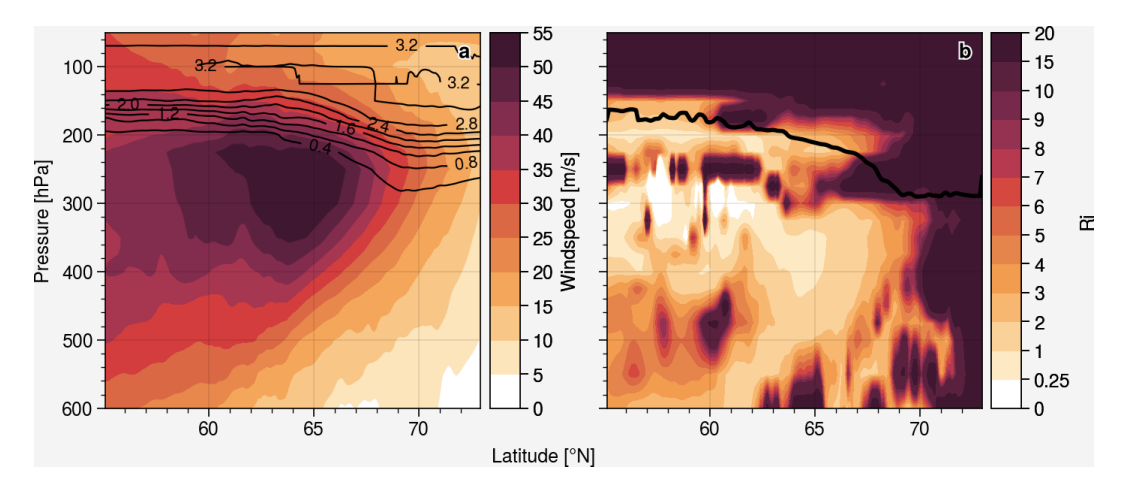


Figure 13. Case 2: (a) CM10 horizontal wind speed, the black contour line show the O_3 -like tracer and (b) gradient Richardson number (Ri), the black line indicates the PV tropopause.

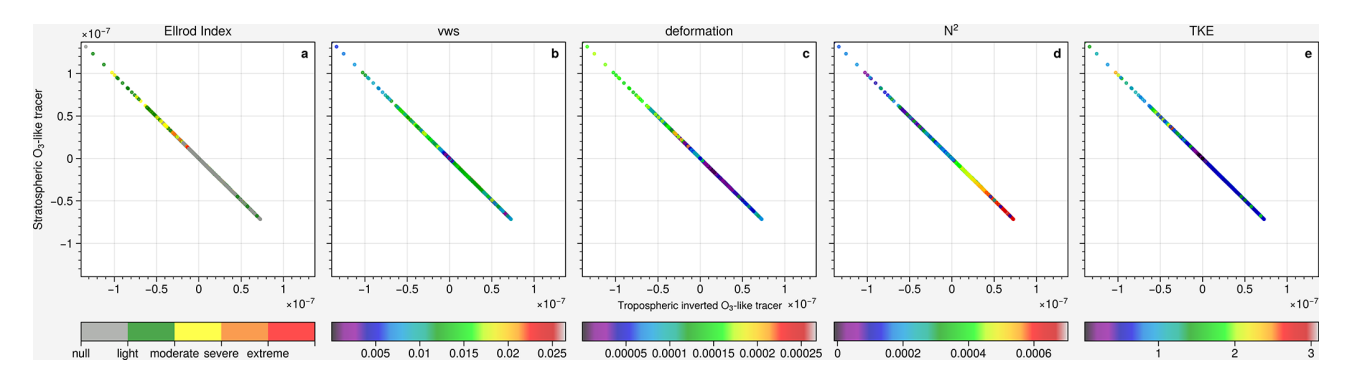


Figure 14. Case 2: delta tracer-tracer correlation of stratospheric O_3 -like/inverted tropospheric O_3 -like tracers (mol mol⁻¹) color-coded with (a) Ellrod index (s⁻²), (b) vertical wind shear (s⁻¹), (c) deformation (s⁻¹), (d) Brunt-Väisälä frequency (s⁻²) and (e) turbulence kinetic energy (m² s⁻²) on 5 February 2016 at 05:00 UTC.

not play much role, proving that the vertical tracer gradient is responsible for the mixing in this case. Case 1 also becomes relatively weaker as expected since the downward mixing is attributed to the tracer gradient. The weakest case 2 turns out to be the strongest case without the impact of the tracer gradient.

To conclude, vertical turbulent mixing by CAT in the model simulations leads to an enhanced and significant tracer mixing in the UTLS region. The strength and direction of the mixing depends on the particular situation, whether the tracer gradient or the dynamic and thermodynamics of the atmosphere play a role. The tracer gradient plays the most important role since mixing will be meaningless if there is no tracer gradient. This confirms the findings of Kaluza et al. (2021) and Kunkel et al. (2019) that strong dynamical forcing like vertical wind shear could lead to mixing even in the stable atmosphere with a typical stratospheric N^2 value.

4 Conclusions

This study presents model simulations for vertical tracer mixing in the UTLS region. The simulation configuration with an enhanced vertical resolution in the UTLS allows a more detailed analysis of turbulent mixing in this region and provides a suitable tool in the future understanding and quantification of the bidirectional cross-tropopause transport with implications on Earth's radiation budget. In this work, a new enhanced vertical resolution model setup (~200 m vertical resolution in the UTLS) for the regional model COSMO, which is nested within the multi-scale climate chemistry model MECO(n), is presented. It performs similar to established configurations and the ERA5 reanalysis with respect to large-scale temperature and humidity fields in the UTLS, but allows a better representation and analysis of turbulent mixing events in this region. Within the relatively short simulation period, the simulations are able to capture several distinct turbulent mixing events in the UTLS with different characteristics including balanced and imbalanced bidirectional

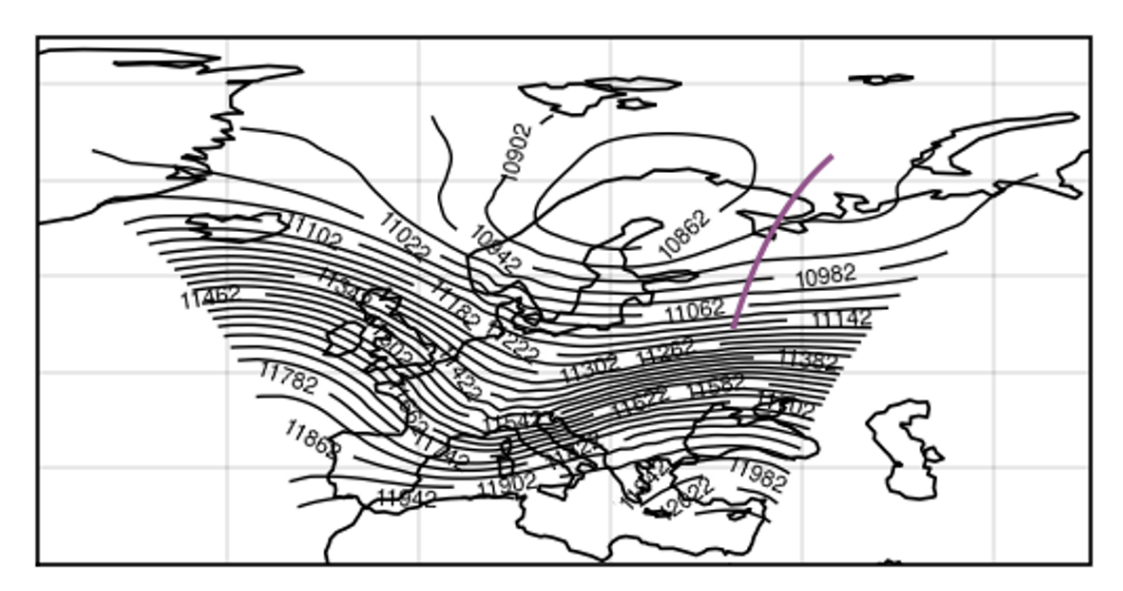


Figure 15. Case 3: geopotential height (gpm) at 200 hPa from CM40 on 3 February 2016 at 22:00 UTC. The purple line indicates the location of the selected cross section of case 3.

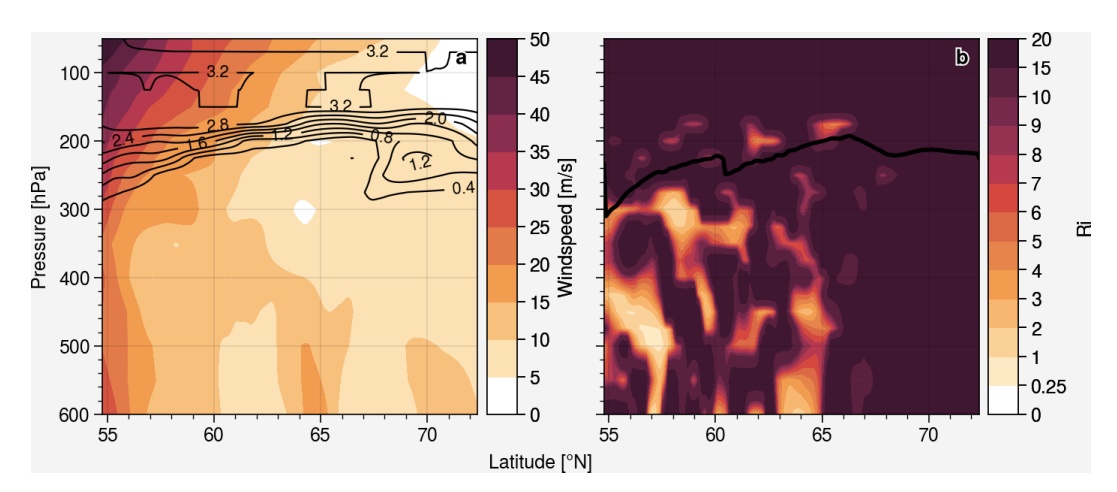


Figure 16. Case 3: (a) CM10 horizontal wind speed, the black contour line show the O_3 -like tracer and (b) gradient Richardson number (Ri), the black line indicates the PV tropopause.

mixing induced by turbulence and strong vertical tracer gradient.

The simulated turbulent kinetic energy (TKE) is spatially and temporally well matched with the (post-simulation) diagnosed Ellrod index, showing the model is able to generate turbulence in the UTLS in agreement with the grid-scale wind field data from the model output. The derived turbulence signal from N_2O also shows a reasonable consistency with the simulated turbulence. However, further comparison with observation is needed considering both the modeled TKE and diagnosed Ellrod index are calculated from the COSMO wind field. This model turbulence is able to significantly mix trace species vertically, as analyzed from the changes in the vertical distribution of passive tracers. However, individual mixing events depend on the particu-

lar weather situation, for example, the vicinity of a jet stream which located near the tropopause experiencing the strongest mixing due to the high vertical wind shear and tracer gradient (case 1). However, it remains challenging to determine how well the model mixing strength is compared to the real world. Further analysis with measurement data is needed when a more comprehensive measurement dataset is available.

The diagnostic of a delta tracer-tracer correlation is used for the analysis of model simulations, in which the correlation of tracer differences between simulations with and without a representation of the turbulent mixing in the UTLS of stratospheric and tropospheric tracers are compared against each other. Both the vertical tracer gradient and the dynamic and thermodynamic forcing, i.e., the stability and stratification, play important roles in the strength of vertical species

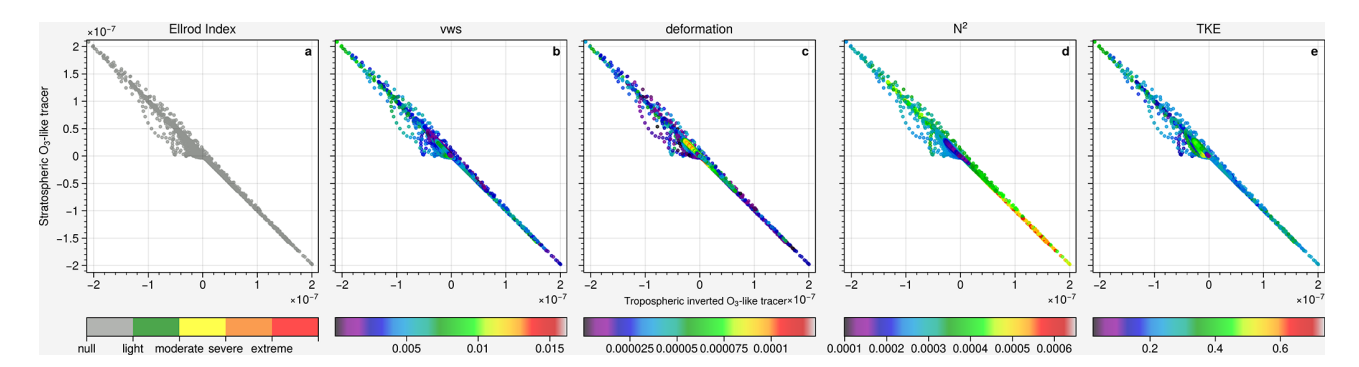


Figure 17. Case 3: delta tracer–tracer correlation of stratospheric O_3 -like/inverted tropospheric O_3 -like tracers (mol mol⁻¹) color-coded with (a) Ellrod index (s⁻²), (b) vertical wind shear (s⁻¹), (c) deformation (s⁻¹), (d) Brunt–Väisälä frequency (s⁻²) and (e) turbulence kinetic energy (m² s⁻²) on 3 February 2016 at 22:00 UTC.

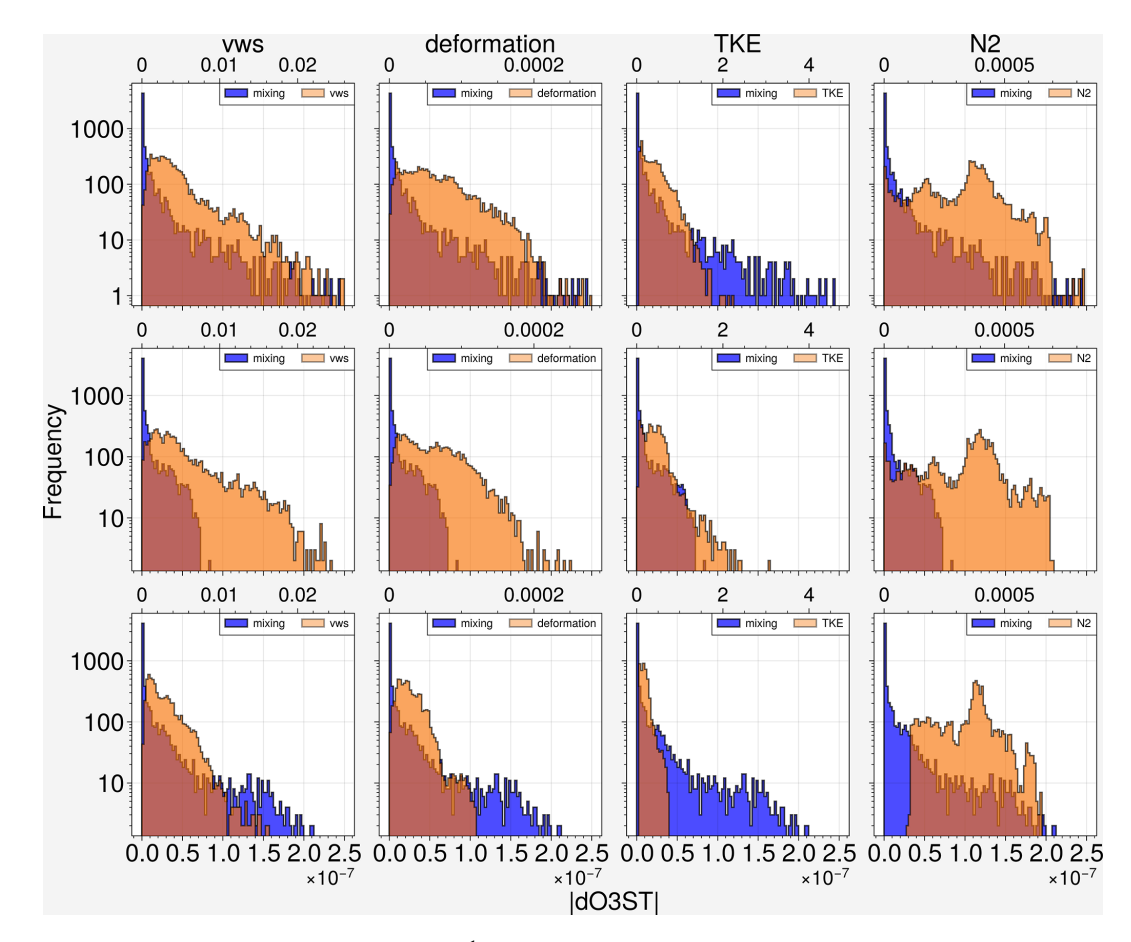


Figure 18. Frequency distribution of $|dO_3ST|$ (mol mol⁻¹) of O_3 -like tracers, vertical wind shear, deformation, TKE and N2 for case 1 (top), case 2 (middle), and case 3 (bottom).

exchange, especially when the vertical wind shear is strong enough to overcome the stable atmosphere. Depending on the individual situation, either the dynamical forcing or pre-existing tracer gradients (or both) can be the dominant drivers for the exchange events. The favorable combination of both factors can lead to an efficient mixing event, maximising tracer exchange fluxes. These events can be irreversible, i.e.,

the exchange of tracers happens along the diagonal of a delta tracer–tracer correlation, leading to a disturbance of typical stratospheric or tropospheric chemical compositions in the respective parts of the atmosphere with implications for climate, e.g., via the radiative impact of exchanged species.

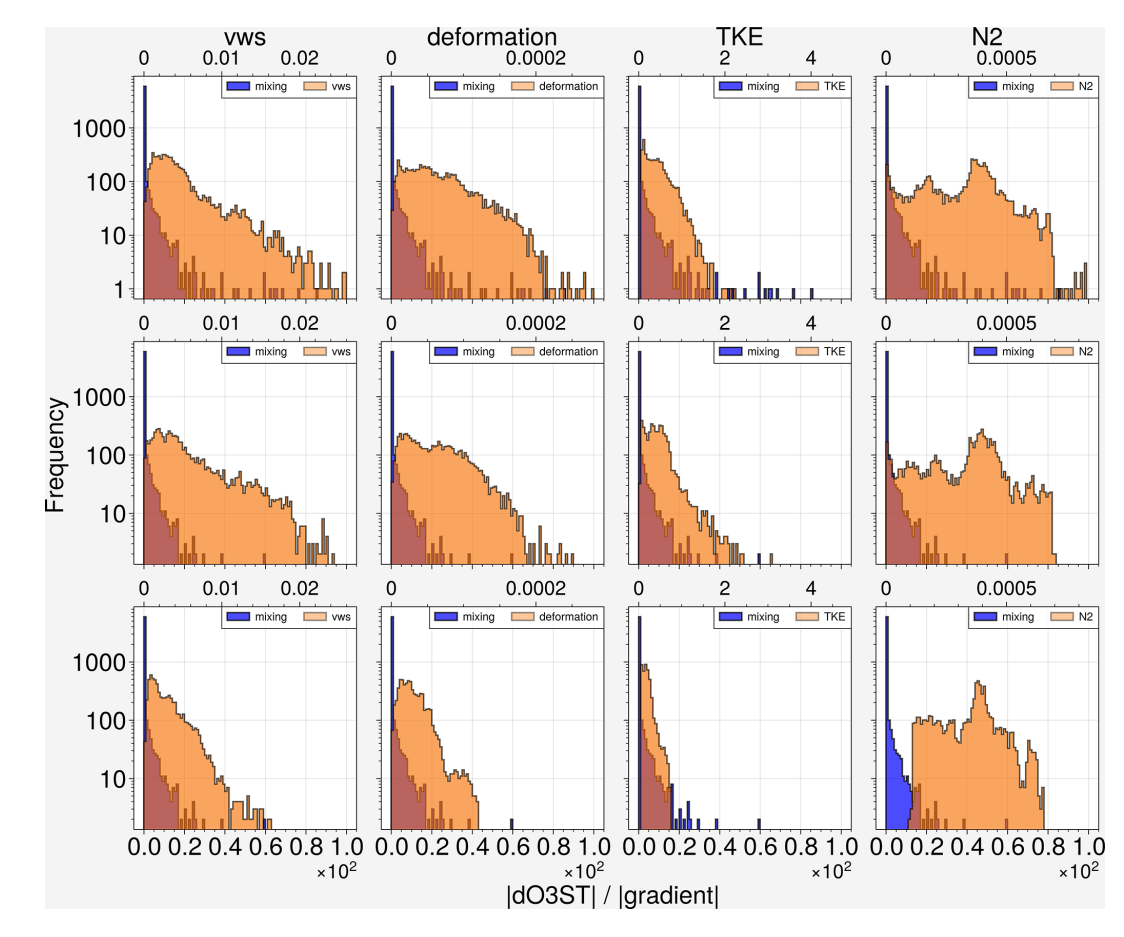


Figure 19. Frequency distribution of $|dO_3ST|/|gradient|$ of O_3 -like tracers, vertical wind shear, deformation, TKE and N2 for case 1 (top), case 2 (middle), and case 3 (bottom).

Code availability. The model code of the MECO(n) system can be obtained by becoming a member of the EMAC consortium as described on the corresponding webpage at https://messy-interface.org (last access: 1 December 2024).

Data availability. Data from this work are available upon request.

Supplement. The supplement related to this article is available online at https://doi.org/10.5194/acp-25-13123-2025-supplement.

Author contributions. CHC and HT conceptualized the study with contributions from PH. CHC performed the simulations and analyzed the model results. The results were interpreted by CHC, HT and PH. CHC wrote the article with significant input from HT and PH.

Competing interests. The contact author has declared that none of the authors has any competing interests.

Disclaimer. Publisher's note: Copernicus Publications remains neutral with regard to jurisdictional claims made in the text, published maps, institutional affiliations, or any other geographical representation in this paper. While Copernicus Publications makes every effort to include appropriate place names, the final responsibility lies with the authors. Also, please note that this paper has not received English language copy-editing. Views expressed in the text are those of the authors and do not necessarily reflect the views of the publisher.

Special issue statement. This article is part of the special issue "The Modular Earth Submodel System (MESSy) (ACP/GMD interjournal SI)". It is not associated with a conference.

Acknowledgements. This work has been funded by the Deutsche Forschungsgemeinschaft (DFG, German Research Foundation) – TRR 301 – Project-ID 428312742 (project B01). The simulations were conducted using the supercomputer MOGON II of Johannes Gutenberg University Mainz.

Financial support. This research has been supported by the Deutsche Forschungsgemeinschaft (grant no. 428312742).

This open-access publication was funded by Johannes Gutenberg University Mainz.

Review statement. This paper was edited by Petr Šácha and reviewed by three anonymous referees.

References

- Baldauf, M., Seifert, A., Förstner, J., Majewski, D., Raschendorfer, M., and Reinhardt, T.: Operational convective-scale numerical weather prediction with the COSMO model: Description and sensitivities, Monthly Weather Review, 139, 3887–3905, https://doi.org/10.1175/MWR-D-10-05013.1, 2011.
- Blackadar, A. K.: The vertical distribution of wind and turbulent exchange in a neutral atmosphere, Journal of Geophysical Research, 67, 3095–3102, https://doi.org/10.1029/JZ067i008p03095, 1962.
- Butchart, N. and Scaife, A.: Removal of chlorofluorocarbons by increased mass exchange between the stratosphere and troposphere in a changing climate, Nature, 410, 799–802, https://doi.org/10.1038/35071047, 2001.
- Dee, D. P., Uppala, S. M., Simmons, A. J., Berrisford, P., Poli, P., Kobayashi, S., Andrae, U., Balmaseda, M. A., Balsamo, G., Bauer, P., Bechtold, P., Beljaars, A. C. M., van de Berg, L., Bidlot, J., Bormann, N., Delsol, C., Dragani, R., Fuentes, M., Geer, A. J., Haimberger, L., Healy, S. B., Hersbach, H., Hólm, E. V., Isaksen, L., Kållberg, P., Köhler, M., Matricardi, M., McNally, A. P., Monge-Sanz, B. M., Morcrette, J.-J., Park, B.-K., Peubey, C., de Rosnay, P., Tavolato, C., Thépaut, J.-N., and Vitart, F.: The ERA-Interim reanalysis: configuration and performance of the data assimilation system, Quarterly Journal of the Royal Meteorological Society, 137, 553–597, https://doi.org/10.1002/qj.828, 2011.
- Doms, G. and Baldauf, M.: A description of the nonhydrostatic regional model COSMO-Model, Part I: Dynamics and Numerics, Deutscher Wetterdienst, Offenbach, (Ed.) U. Schättler, https://doi.org/10.5676/DWD_pub/nwv/cosmo-doc_6.00_I, 2018.
- Doms, G., Förstner, J., Heise, E., Herzog, H.-J., Mironov, D., Raschendorfer, M., Reinhardt, T., Ritter, B., Schrodin, R., Schulz, J.-P., and Vogel, G.: Consortium for small-scale modelling a description of the nonhydrostatic regional COSMO-model part II physical parameterizations, Deutscher Wetterdienst, https://doi.org/10.5676/DWD_pub/nwv/cosmo-doc_5.05_II, 2018.
- Dutton, J. A. and Panofsky, H. A.: Clear air turbulence: a mystery may be unfolding, Science, 167, 937–944, https://doi.org/10.1126/science.167.3920.937, 1970.
- Eckstein, J., Schmitz, S., and Ruhnke, R.: Reaching the lower stratosphere: validating an extended vertical grid for COSMO, Geosci. Model Dev., 8, 1839–1855, https://doi.org/10.5194/gmd-8-1839-2015, 2015.
- Ellrod, G., Lester, P., and Ehernberger, L.: Clear air turbulence, in: Encyclopedia of Atmospheric Sciences, 393–403, ISBN 978-0-

- 12-227090-1, https://doi.org/10.1016/B0-12-227090-8/00104-4, 2003
- Ellrod, G. P. and Knapp, D. I.: An objective clear-air turbulence forecasting technique: Verification and operational use, Weather and Forecasting, 7, 150–165, https://doi.org/10.1175/1520-0434(1992)007<0150:AOCATF>2.0.CO;2, 1992.
- Ellrod, G. P. and Knox, J. A.: Improvements to an operational clear-air turbulence diagnostic index by addition of a divergence trend term, Weather and Forecasting, 25, 789–798, https://doi.org/10.1175/2009WAF2222290.1, 2010.
- Esler, J. G. and Polvani, L. M.: Kelvin–helmholtz instability of potential vorticity layers: a route to mixing, Journal of the Atmospheric Sciences, 61, 1392–1405, https://doi.org/10.1175/1520-0469(2004)061<1392:KIOPVL>2.0.CO;2, 2004.
- Forster, P., Storelvmo, T., Armour, K., Collins, W., Dufresne, J.-L., Frame, D., Lunt, D., Mauritsen, T., Palmer, M., Watanabe, M., Wild, M., and Zhang, H.: Chapter 7: The Earth's energy budget, climate feedbacks, and climate sensitivity, Climate Change 2021: The Physical Science Basis. Contribution of Working Group I to the Sixth Assessment Report of the Intergovernmental Panel on Climate Change, https://doi.org/10.25455/wgtn.16869671.v1, 2021.
- Forster, P. M. and Shine, K. P.: Radiative forcing and temperature trends from stratospheric ozone changes, Journal of Geophysical Research-Atmospheres, 102, 10841–10855, https://doi.org/10.1029/96JD03510, 1997.
- Forster, P. M. and Shine, K. P.: Stratospheric water vapour changes as a possible contributor to observed stratospheric cooling, Geophysical Research Letters, 26, 3309–3312, https://doi.org/10.1029/1999GL010487, 1999.
- Forster, P. M. d. F. and Shine, K. P.: Assessing the climate impact of trends in stratospheric water vapor, Geophysical Research Letters, 29, 10-1–10-4, https://doi.org/10.1029/2001GL013909, 2002.
- Gettelman, A., Hoor, P., Pan, L. L., Randel, W. J., Hegglin, M. I., and Birner, T.: The extratropical upper troposphere and lower stratosphere, Reviews of Geophysics, 49, https://doi.org/10.1029/2011RG000355, 2011.
- Giorgetta, M. A., Manzini, E., Roeckner, E., Esch, M., and Bengtsson, L.: Climatology and forcing of the quasi-biennial oscillation in the MAECHAM5 model, Journal of Climate, 19, 3882–3901, https://doi.org/10.1175/JCLI3830.1, 2006.
- Holton, J. R., Haynes, P. H., McIntyre, M. E., Douglass, A. R., Rood, R. B., and Pfister, L.: Stratosphere-troposphere exchange, Reviews of Geophysics, 33, 403–439, https://doi.org/10.1029/95RG02097, 1995.
- Hu, B., Tang, J., Ding, J., and Liu, G.: Regional down-scaled future change of clear-air turbulence over East Asia under RCP8.5 scenario within the CORDEX-EA-II project, International Journal of Climatology, 41, 5022–5035, https://doi.org/10.1002/joc.7114, 2021.
- Jaeger, E. B. and Sprenger, M.: A Northern Hemispheric climatology of indices for clear air turbulence in the tropopause region derived from ERA40 reanalysis data, Journal of Geophysical Research-Atmospheres, 112, https://doi.org/10.1029/2006JD008189, 2007.
- Jeuken, A. B. M., Siegmund, P. C., Heijboer, L. C., Feichter, J., and Bengtsson, L.: On the potential of assimilating meteorological analyses in a global climate model for the purpose of model

- validation, Journal of Geophysical Research-Atmospheres, 101, 16939–16950, https://doi.org/10.1029/96JD01218, 1996.
- Jöckel, P., Sander, R., Kerkweg, A., Tost, H., and Lelieveld, J.: Technical Note: The Modular Earth Submodel System (MESSy)
 a new approach towards Earth System Modeling, Atmos. Chem. Phys., 5, 433–444, https://doi.org/10.5194/acp-5-433-2005, 2005.
- Jöckel, P., Tost, H., Pozzer, A., Brühl, C., Buchholz, J., Ganzeveld, L., Hoor, P., Kerkweg, A., Lawrence, M. G., Sander, R., Steil, B., Stiller, G., Tanarhte, M., Taraborrelli, D., van Aardenne, J., and Lelieveld, J.: The atmospheric chemistry general circulation model ECHAM5/MESSy1: consistent simulation of ozone from the surface to the mesosphere, Atmos. Chem. Phys., 6, 5067–5104, https://doi.org/10.5194/acp-6-5067-2006, 2006.
- Jöckel, P., Kerkweg, A., Buchholz-Dietsch, J., Tost, H., Sander, R., and Pozzer, A.: Technical Note: Coupling of chemical processes with the Modular Earth Submodel System (MESSy) submodel TRACER, Atmos. Chem. Phys., 8, 1677–1687, https://doi.org/10.5194/acp-8-1677-2008, 2008.
- Jöckel, P., Kerkweg, A., Pozzer, A., Sander, R., Tost, H., Riede, H., Baumgaertner, A., Gromov, S., and Kern, B.: Development cycle 2 of the Modular Earth Submodel System (MESSy2), Geosci. Model Dev., 3, 717–752, https://doi.org/10.5194/gmd-3-717-2010, 2010.
- Kaluza, T., Kunkel, D., and Hoor, P.: On the occurrence of strong vertical wind shear in the tropopause region: a 10-year ERA5 northern hemispheric study, Weather Clim. Dynam., 2, 631–651, https://doi.org/10.5194/wcd-2-631-2021, 2021.
- Keller, J. L.: Clear air turbulence as a response to mesoand synoptic-scale dynamic processes, Monthly Weather Review, 118, 2228–2243, https://doi.org/10.1175/1520-0493(1990)118<2228:CATAAR>2.0.CO;2, 1990.
- Kerkweg, A. and Jöckel, P.: The 1-way on-line coupled atmospheric chemistry model system MECO(n) Part 2: On-line coupling with the Multi-Model-Driver (MMD), Geosci. Model Dev., 5, 111–128, https://doi.org/10.5194/gmd-5-111-2012, 2012a.
- Kerkweg, A. and Jöckel, P.: The 1-way on-line coupled atmospheric chemistry model system MECO(n) Part 1: Description of the limited-area atmospheric chemistry model COSMO/MESSy, Geosci. Model Dev., 5, 87–110, https://doi.org/10.5194/gmd-5-87-2012, 2012b.
- Kerkweg, A., Hofmann, C., Jöckel, P., Mertens, M., and Pante, G.: The on-line coupled atmospheric chemistry model system MECO(n) Part 5: Expanding the Multi-Model-Driver (MMD v2.0) for 2-way data exchange including data interpolation via GRID (v1.0), Geosci. Model Dev., 11, 1059–1076, https://doi.org/10.5194/gmd-11-1059-2018, 2018.
- Kunkel, D., Hoor, P., Kaluza, T., Ungermann, J., Kluschat, B., Giez, A., Lachnitt, H.-C., Kaufmann, M., and Riese, M.: Evidence of small-scale quasi-isentropic mixing in ridges of extratropical baroclinic waves, Atmos. Chem. Phys., 19, 12607–12630, https://doi.org/10.5194/acp-19-12607-2019, 2019.
- Lachnitt, H.-C., Hoor, P., Kunkel, D., Bramberger, M., Dörnbrack, A., Müller, S., Reutter, P., Giez, A., Kaluza, T., and Rapp, M.: Gravity-wave-induced cross-isentropic mixing: a DEEPWAVE case study, Atmos. Chem. Phys., 23, 355–373, https://doi.org/10.5194/acp-23-355-2023, 2023.
- Lacis, A. A., Wuebbles, D. J., and Logan, J. A.: Radiative forcing of climate by changes in the vertical distribution of ozone,

- Journal of Geophysical Research-Atmospheres, 95, 9971–9981, https://doi.org/10.1029/JD095iD07p09971, 1990.
- Lelieveld, J. and Dentener, F. J.: What controls tropospheric ozone?, Journal of Geophysical Research-Atmospheres, 105, 3531–3551, https://doi.org/10.1029/1999JD901011, 2000.
- Meloen, J., Siegmund, P., van Velthoven, P., Kelder, H., Sprenger,
 M., Wernli, H., Kentarchos, A., Roelofs, G., Feichter, J., Land,
 C., Forster, C., James, P., Stohl, A., Collins, W., and Cristofanelli,
 P.: Stratosphere-troposphere exchange: A model and method intercomparison, Journal of Geophysical Research-Atmospheres,
 108, https://doi.org/10.1029/2002JD002274, 2003.
- Mertens, M., Kerkweg, A., Jöckel, P., Tost, H., and Hofmann, C.: The 1-way on-line coupled model system MECO(n) Part 4: Chemical evaluation (based on MESSy v2.52), Geosci. Model Dev., 9, 3545–3567, https://doi.org/10.5194/gmd-9-3545-2016, 2016.
- Miyazaki, K., Watanabe, S., Kawatani, Y., Tomikawa, Y., Takahashi, M., and Sato, K.: Transport and mixing in the extratropical tropopause region in a high-vertical-resolution GCM. Part I: Potential vorticity and heat budget analysis, Journal of the Atmospheric Sciences, 67, 1293–1314, https://doi.org/10.1175/2009JAS3221.1, 2010.
- Muller, E.: Turbulent flux parameterization in a regional-scale model, phd, ECMWF, Shinfield Park, Reading, 193–220, 1981.
- Muñoz-Esparza, D., Sharman, R. D., and Trier, S. B.: On the consequences of PBL scheme diffusion on UTLS wave and turbulence representation in high-resolution NWP models, Monthly Weather Review, 148, 4247–4265, https://doi.org/10.1175/MWR-D-20-0102.1, 2020.
- Overeem, A.: Verification of clear-air turbulence forecasts, Citeseer, https://cdn.knmi.nl/knmi/pdf/bibliotheek/knmipubTR/TR244.pdf, 2002.
- Randel, W. J., Wu, F., and Forster, P.: The extratropical tropopause inversion layer: Global observations with GPS data, and a radiative forcing mechanism, Journal of the Atmospheric Sciences, 64, 4489–4496, https://doi.org/10.1175/2007JAS2412.1, 2007.
- Riese, M., Ploeger, F., Rap, A., Vogel, B., Konopka, P., Dameris, M., and Forster, P.: Impact of uncertainties in atmospheric mixing on simulated UTLS composition and related radiative effects, Journal of Geophysical Research-Atmospheres, 117, https://doi.org/10.1029/2012JD017751, 2012.
- Roeckner, E., Bäuml, G., Bonaventura, L., Brokopf, R., Esch, M., Giorgetta, M., Hagemann, S., Kirchner, I., Kornblueh, L., Manzini, E., Schlese, U., and Schulzweida, U.: The atmospheric general circulation model ECHAM 5. PART I: Model description, Max-Planck-Institut für Meteorologie, https://pure.mpg.de/pubman/faces/ViewItemOverviewPage.jsp?itemId=item_995269, 2003.
- Schättler, U., Doms, G., and Schraff, C.: Consortium for small-scale modelling a description of the nonhydrostatic regional COSMO-model part VII: User's guide, Deutscher Wetterdienst, Offenbach, https://doi.org/10.5676/DWD_pub/nwv/cosmo-doc_6.00_VII, 2021.
- Shapiro, M. A.: Turbulent mixing within tropopause folds as a mechanism for the exchange of chemical constituents between the stratosphere and troposphere, Journal of Atmospheric Sciences, 37, 994–1004, https://doi.org/10.1175/1520-0469(1980)037<0994:TMWTFA>2.0.CO;2, 1980.

- Sharman, R., Tebaldi, C., Wiener, G., and Wolff, J.: An integrated approach to mid- and upper-level turbulence forecasting, Weather and Forecasting, 21, 268–287, https://doi.org/10.1175/WAF924.1, 2006.
- Smith, I. H., Williams, P. D., and Schiemann, R.: Clear-air turbulence trends over the North Atlantic in high-resolution climate models, Climate Dynamics, 61, 1–17, 2023.
- Sprenger, M. and Wernli, H.: A northern hemispheric climatology of cross-tropopause exchange for the ERA15 time period (1979–1993), Journal of Geophysical Research-Atmospheres, 108, https://doi.org/10.1029/2002JD002636, 2003.
- Stohl, A., Bonasoni, P., Cristofanelli, P., Collins, W., Feichter, J., Frank, A., Forster, C., Gerasopoulos, E., Gäggeler, H., James, P., Kentarchos, T., Kromp-Kolb, H., Krüger, B., Land, C., Meloen, J., Papayannis, A., Priller, A., Seibert, P., Sprenger, M., Roelofs, G. J., Scheel, H. E., Schnabel, C., Siegmund, P., Tobler, L., Trickl, T., Wernli, H., Wirth, V., Zanis, P., and Zerefos, C.: Stratosphere-troposphere exchange: A review, and what we have learned from STAC-CATO, Journal of Geophysical Research-Atmospheres, 108, https://doi.org/10.1029/2002JD002490, 2003a.
- Stohl, A., Wernli, H., James, P., Bourqui, M., Forster, C., Liniger, M. A., Seibert, P., and Sprenger, M.: A new perspective of stratosphere–troposphere exchange, Bulletin of the American Meteorological Society, 84, 1565–1574, https://doi.org/10.1175/BAMS-84-11-1565, 2003b.
- Storer, L. N., Williams, P. D., and Joshi, M. M.: Global response of clear-air turbulence to climate change, Geophysical Research Letters, 44, 9976–9984, https://doi.org/10.1002/2017GL074618, 2017

- Traub, M. and Lelieveld, J.: Cross-tropopause transport over the eastern Mediterranean, Journal of Geophysical Research-Atmospheres, 108, https://doi.org/10.1029/2003JD003754, 2003.
- van Velthoven, P. F. J. and Kelder, H.: Estimates of stratosphere-troposphere exchange: Sensitivity to model formulation and horizontal resolution, Journal of Geophysical Research-Atmospheres, 101, 1429–1434, https://doi.org/10.1029/95JD03407, 1996.
- Watkins, C. and Browning, K.: The detection of clear air turbulence by radar, Physics in Technology, 4, 28, https://doi.org/10.1088/0305-4624/4/1/101, 1973.
- Williams, P. D.: Increased light, moderate, and severe clear-air turbulence in response to climate change, Advances in Atmospheric Sciences, 34, 576–586, 2017.
- Williams, P. D. and Joshi, M. M.: Intensification of winter transatlantic aviation turbulence in response to climate change, Nature Climate Change, 3, 644–648, 2013.
- Witschas, B., Gisinger, S., Rahm, S., Dörnbrack, A., Fritts, D. C., and Rapp, M.: Airborne coherent wind lidar measurements of the momentum flux profile from orographically induced gravity waves, Atmos. Meas. Tech., 16, 1087–1101, https://doi.org/10.5194/amt-16-1087-2023, 2023.
- Wolff, J. K. and Sharman, R. D.: Climatology of upper-level turbulence over the contiguous united states, Journal of Applied Meteorology and Climatology, 47, 2198–2214, https://doi.org/10.1175/2008JAMC1799.1, 2008.